

Review of Land-Atmosphere-Cloud Coupling in Observations and Models

Alan Betts, Atmospheric Research, Pittsford, VT, USA

Abstract: This is a summary of my two review papers (Betts 2004; 2009) that outlines the development of my understanding of land-atmosphere-cloud coupling over the past decade.

Keywords: Hydrometeorology, land-surface, cloud radiative forcing, surface albedo, evaporative fraction, soil moisture, diurnal cycle

Understanding hydrometeorology using global models (Betts 2004)

This review used global model data to propose a new framework for understanding the land-surface coupling in global models between soil moisture, cloud base and cloud cover, the radiation fields, the surface energy partition, evaporation and precipitation. I had worked extensively with data from land-surface field experiments in the Konza grassland prairie in Kansas (Betts and Ball 1998) and the Canadian boreal forest (Betts et al. 1999; 2001). I had also developed idealized ‘equilibrium’ mixed layer models which averaged over the diurnal cycle over land (Betts 2000; Betts et al. 2004; Betts and Chiu 2010); and studied the energy and water budgets of river basins using reanalysis data (Betts et al. 1999). So when I was asked to give the 2004 American Meteorological Society Horton lecture in hydrology, I decided to take a closer look at the coupling of land-surface processes and hydrometeorology in the European Centre model used for their 40-year reanalysis (ERA40). Here I will show just three figures (out of eighteen), which confirmed concepts I had been developing, and suggested new avenues for research. But first I will outline my frame of reference, quoting from Betts (2004, pp.1673-1674)

The title of this paper is meant to be a paradox. Usually we rely on simple models to gain understanding, but hydrometeorology is too complex for that, and too important for us to be satisfied with rough approximations. The climate interactions of water (vapor, liquid and ice, and its phase change and radiation interactions) are everywhere, and they are central to and closely coupled to life, and to understanding climate change. Climate is both local and global: we need earth system models to understand the coupled system that we observe. Only with models can we try to both fit the parts together, and then take them apart again to see what matters, and where. It is true that global models are such a challenge to construct, code, and debug; that when they run, producing something closely resembling the climate of the earth, the temptation is to sit back with relief. We run ensembles for weather forecasting and climate scenarios, talk about the complexities of cloud feedback and publish papers, and forward the results to the public and those in power to address questions of pressing political importance. But, we have to do much better—we must understand how well the models represent physical processes and feedbacks.

After a couple of decades of studying convection in the Tropics, moist thermodynamics, and climate using simple models, I realized about 15 years ago that improving our global models was essential to understanding the earth system. I have spent considerable effort since evaluating global models using high quality field data (Betts et al. 1996), primarily from land surface experiments from land surface experiments such as the First International Satellite Land Surface Climatology Project (ISLSCP) Field Experiment (FIFE), Boreal Ecosystem–Atmosphere Study (BOREAS), and Large-Scale Biosphere–Atmosphere Experiment (LBA); and it is this that drew me into hydrometeorology. Along the way, however, I have realized that global models can be used as tools to understand interacting processes. Using global models in this way is also useful, because it forces us to contrast our model world, which we dimly understand because at least we wrote the equations, with the real world, where we only understand fragments of a complex living system.

Coupling of soil moisture to the lifting condensation level (LCL)

The ERA40 global model was run in seasonal forecast mode for 120 days, initialized on 1 May, 1987 with two idealized soil moisture configurations: one with soil moisture index, $SMI = 1$, a wet initialization at field capacity,

and one dry initialization with $SMI = 0.25$ for vegetated areas. $SMI-L1$ for soil layer 1 (0-7cm) is scaled to run from zero to one

$$SMI-L1 = (SM - 0.171)/(0.323 - 0.171) \quad (1)$$

where SM is the model soil water fraction, the model soil permanent wilting point is 0.171 and the model field capacity is 0.323. Omitting the first 5 days of the forecasts, 5-day means were generated for regions of the continents in mid-latitudes and the tropics. Away from the monsoons, there were big differences in regional precipitation and evaporation between wet and dry simulations, as noted earlier in Beljaars et al. (1996).

P_{LCL} , the pressure height of the lifting condensation level (LCL) is a useful measure of the LCL, because it can be computed easily from parcel T and surface pressure p , as

$$P_{LCL} = p - p^* \quad (2)$$

where p^* is the parcel *saturation pressure*: the pressure at the LCL, when a parcel lifted dry adiabatically reaches water vapor saturation. Saturation temperature and pressure (T^* , p^*) define the properties conserved in reversible adiabatic processes (Betts 1982), and the properties of parcels as they cross cloud boundaries. Over land, when there are boundary layer (BL) clouds in the afternoon, P_{LCL} gives a good estimate of mixed layer depth.

Figure 1 merges both wet and dry simulations for three regions of the Americas, showing that as the seasonal forecasts dry down, there is a relatively tight coupling between SMI for the top 0-7cm soil layer and the pressure height of the LCL. Why such a tight relation across latitude and different vegetation regimes? In the model formulation, transpiration dominates in vegetated areas, and stomatal conductance/resistance, which drops saturation across the (model) leaf surface, determines the equilibrium of relative humidity, RH , over land, and RH is closely linked to the saturation pressure of the LCL (next section). This is the fundamental difference between the land and ocean, where there is saturation at the ocean surface (rather than inside the leaf). Over the ocean, the drop in saturation above the sea surface is related only to the mixing down of less saturated air from above the convective boundary layer (CBL) (see Betts and Ridgway 1989). Over land both this process and stomatal conductance are involved. I had seen the impact of this coupling in equilibrium models of the land BL (Betts 2000; Betts et al. 2003), so I was not surprised to see it in the ERA40 model.

But this is a two-way coupling. When conditions are moist, and cloud-base is low, it rains more, and falling rain evaporates into the BL, lowering the cloud-base saturation level, and rain increases the first layer soil moisture (see Figure 11, later).

Relation of RH to LCL

The thermodynamic coupling of Z_{LCL} (the height of the LCL) and P_{LCL} to parcel RH , T and pressure, P , are shown in Figure 2. The left panel shows Z_{LCL} as a function of temperature (the dependence on pressure is negligible in the lower troposphere), and the right panel shows that the ratio P_{LCL}/p has only a weak dependence of T . The means that relative humidity and the pressure height of mean cloud-base are very closely linked.

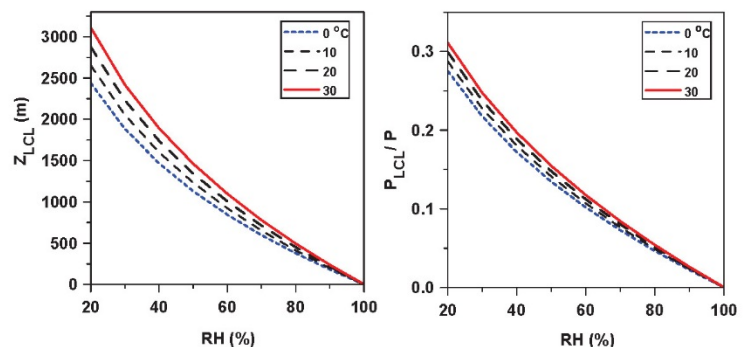


Figure 2: Relation between RH and Z_{LCL} and P_{LCL} as a function of parcel T , p . (Betts 2009)

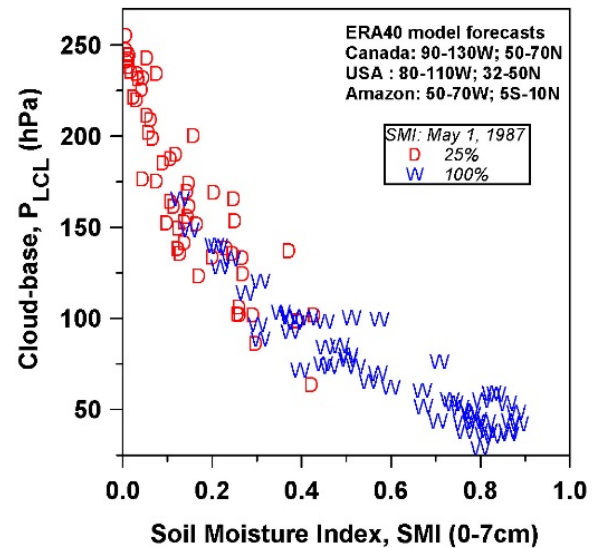


Figure 1: Coupling between SMI and the pressure height of the LCL for three regions of the Americas. (Betts 2004)

Coupling between P_{LCL} , the surface fluxes and the surface meteorology

Figures 1 and 2 show that soil moisture, cloud-base, represented by P_{LCL} , and RH are all coupled. Figure 3 summarizes the coupling between P_{LCL} , the surface fluxes and the surface 2-m meteorology for just the Amazon region from these same 120-day forecasts from 1 May, 1987. The wet and dry simulations simply merge to show quasi-linear relationships between P_{LCL} and (left) the surface sensible and latent heat fluxes, H and λE , and (right) 2-m temperature and specific humidity, T_2 and Q_2 . The dashed lines are a fit from the equilibrium model of Betts et al. (2004) showing the general consistency between an idealized model, which averages over the diurnal cycle, and the 5-day means from ERA40. So the local climatology of the fully coupled global model, with all its complexity, shows a relatively tight and conceptually simple coupling between the surface fluxes and the surface meteorology on daily and longer timescales. Our analysis of the Canadian Prairie data took this as a starting point.

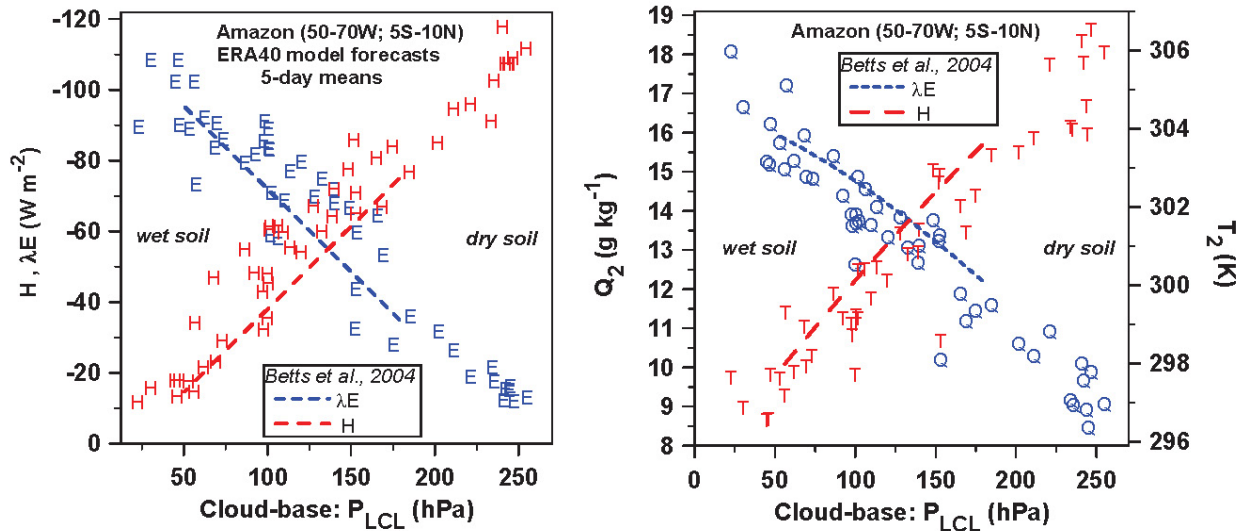


Figure 3. Coupling between P_{LCL} , the surface fluxes and the 2-m meteorology for the Amazon. (Betts 2004)

Coupling between diurnal cycle of temperature and longwave radiation.

When I explored the links with the diurnal temperature range (DTR) and the radiative fluxes using daily ERA40 reanalysis means for river basins, I was surprised to find that the tightest link was between DTR and the daily mean net longwave, LW_n . This is a good example of how coupled models can surprise us and help us understand processes. The fall of temperature from maximum to minimum is of course related to LW_n . We are familiar with this in the conditions that gives us the first frost in the fall on clear nights. However its importance to the equilibrium surface climate was not appreciated because most research on the factors affecting DTR focused on the daytime solar forcing, and the daytime surface energy partition related to water availability. Subsequently, Betts (2006) explored further the forcing of the diurnal cycle and the strength of the night-time BL by LW_n using ERA40 river basin data. The Canadian Prairie data show that this tight LW coupling is a characteristic of the warm season with no surface snow cover.

Figure 4 shows this coupling for thirty years of daily mean data averaged over the Madeira River basin in the

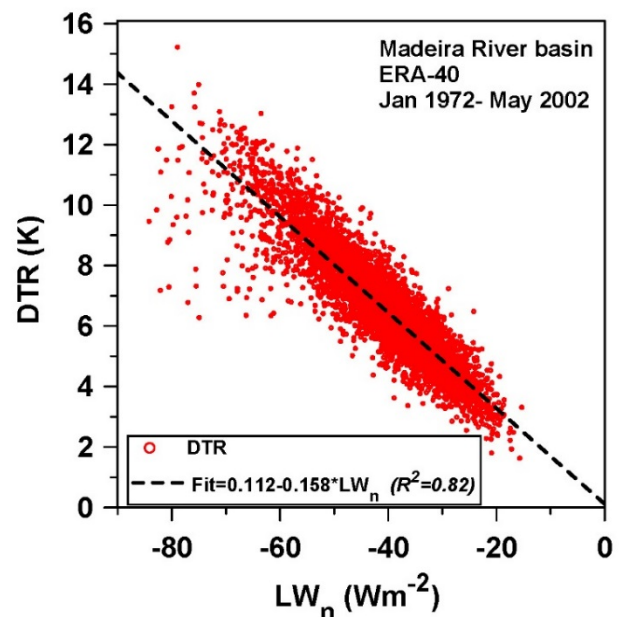


Figure 4. Coupling between DTR and LW_n . (Betts 2004)

SW Amazon. The linear fit to the daily means has $R^2 = 0.82$. Of course, the equilibrium climate over land must satisfy both daytime and night-time constraints. It is primarily cloud cover that determines the daily variability of LW_n and net shortwave (SW_n), and we will return to this using the Canadian Prairie data. The big issue for models is whether clouds in a given model have the correct impact on the surface radiation budget: otherwise the land-surface mean and diurnal climate will be biased.

Land-surface-atmosphere coupling in observations and models (Betts 2009)

We have selected some important examples from this second review. The first is the role of the surface albedo and the effective cloud albedo on the shortwave and longwave fluxes. The second is how RH and cloud are coupled to surface LW_n (which we have shown is coupled to DTR). The third is the dependence of the surface energy partition on soil water, and vector methods for understanding mixed layer evolution. We then revisit the soil water, evaporative fraction, cloud-base links; and discuss how net radiation (R_n) depends on cloud forcing while evaporative fraction depends on soil moisture. Finally we show that the ratio of the shortwave cloud radiative forcing to the precipitation forcing has a low bias in ERA40.

Importance of surface albedo and snow cover

Snow covered grassland has a radically different surface energy budget (SEB) from conifers (Betts and Ball 1997), where the trees shade the snow. Figure 5 illustrates this using data from the boreal forest. With snow cover, grass has a surface albedo $\alpha_{surf} \approx 0.7$ to 0.8 , much higher than deciduous aspen (≈ 0.25), which in turn is higher than conifers (≈ 0.15) (left panel). In March, this leads to near-zero R_n over grassland (right panel), and a substantial R_n over the forest (which increases as the solar zenith angle decreases during March). The high albedo of the snow covered Canadian Prairies has a very large impact on the cold season climate (see following chapter).

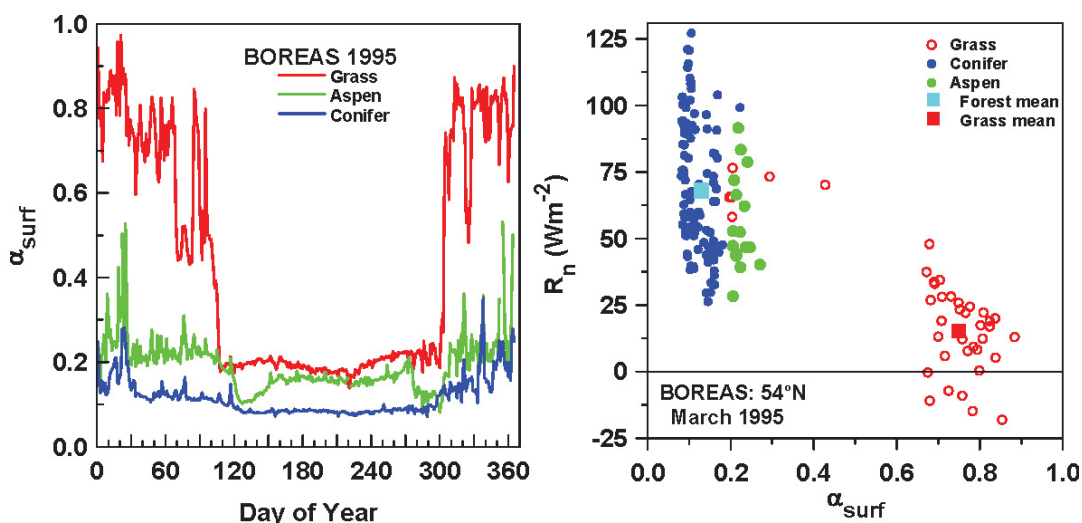


Figure 5. Surface albedo of conifer, aspen and grass (left); March R_n as a function of surface albedo (right). (Betts 2009)

In numerical models, errors in the surface albedo with snow propagate into the model forecast. In 1996, the ECMWF model had grassland albedos with snow (≈ 0.8) over the boreal forest, which gave the large errors in the 5-day forecasts of the 850hPa temperature, shown in Figure 6 (left). In 1997 the boreal forest albedo was reduced to ≈ 0.2 with snow, and these systematic errors largely disappeared (Viterbo and Betts 1999). An improved snow model was then developed (Van den Hurk et al. 2000).

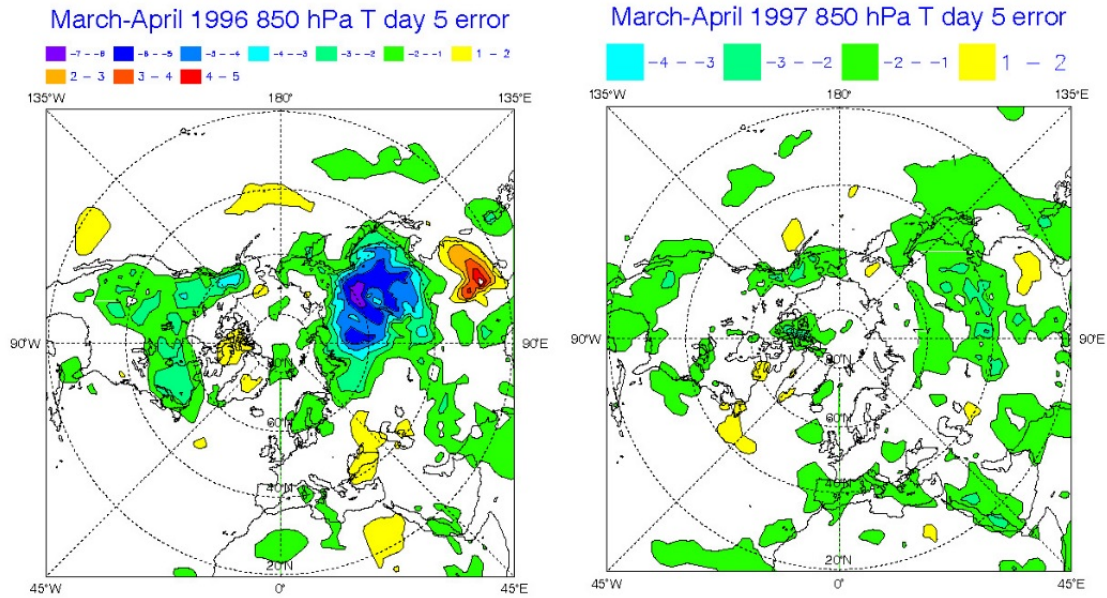


Figure 6. Mean 5-day 850 hPa forecasts temperature error for March-April, 1996 and March-April, 1997. (Betts 2009)

Concept of Effective Cloud Albedo

Like snow, clouds also strongly reflect SW radiation, and we can define the net shortwave cloud forcing ($SWCF_n$) as the difference between SW_n and the corresponding net clear-sky flux, SWC_n

$$SWCF_n = SW_n - SWC_n \quad (3)$$

The effective cloud albedo (ECA) is a normalized $SWCF_n$

$$ECA = -SWCF_n / SWC_n \quad (4)$$

Then the surface SW_n can be derived from the downwelling clear-sky flux,

$$SW_n = (1 - \alpha_{surf})(1 - ECA) SWC_{dn} \quad (5)$$

This formulation shows that the surface and the effective cloud albedos play a symmetric role in reducing the clear-sky downwelling flux.

This transformation from $SWCF_n$ to effective cloud albedo is illustrated in Figure 7. The envelope of red points are the daily clear sky SW_n fluxes from ERA40 for the Ohio-Tennessee river basin for the five years, 1996-2000 (Betts 2007). The blue dots are the daily-mean all-sky SW_n fluxes. The transformation given by (3) and (4) gives us the right-hand panel of the daily mean ECA, scaled between 0 and 1. Note the wide scatter on the daily time-scale,

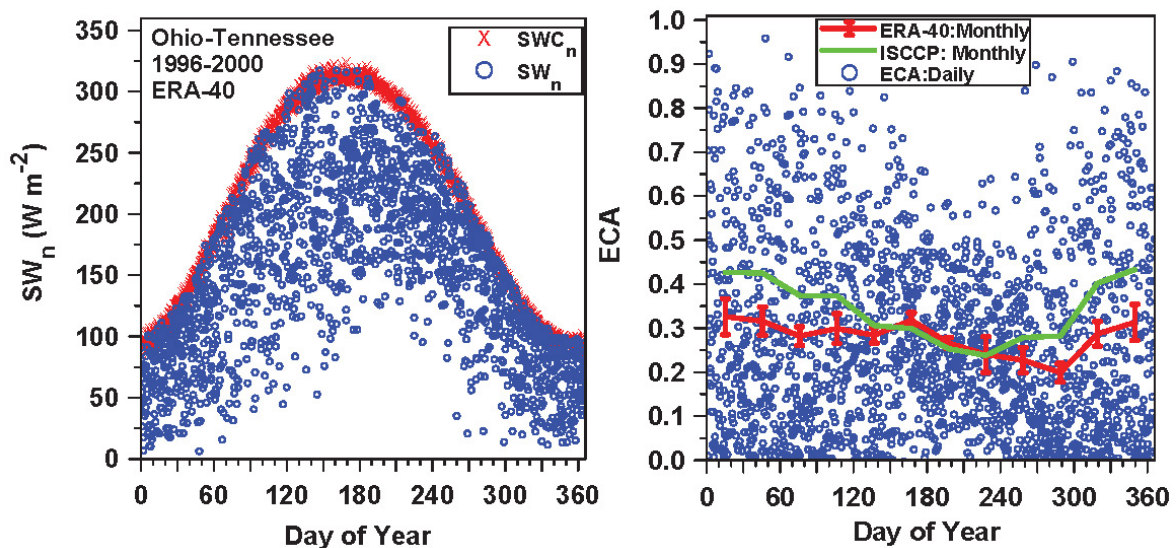


Figure 7. Daily-mean SWC_n (clear) and SW_n for Ohio-Tennessee river basin (left) and transformation to effective cloud albedo (right). (Betts 2009)

associated with atmospheric processes that generate clouds: much more daily variability than in the surface albedo. But there is some mean seasonal structure here. The solid curves show the monthly means for this period for ERA40 (red) and the International Satellite Cloud Climatology Project (ISCCP) data (green). Except in summer, ERA40 has too little reflective cloud. The error bars are the interannual variability of the bias, ERA40-ISCCP, showing that, although cloud cover is a noisy variable on the daily timescale, the mean bias of ERA40 is significant. From a climate and a SEB perspective, we see from (5) that a 10% error in ECA is just as significant as a 10% error in the surface albedo.

Dependence of surface LW_n on relative humidity and clouds

The surface LW_n plays a fundamental role in land-atmosphere coupling. The upward and downward LW fluxes are strong functions of temperature. However, on daily-mean timescales in the warm season LW_n is largely determined by humidity and cloud cover. Probably this is because there is typically strong vertical coupling of the atmospheric temperature and moisture structure. For example, the depth of the daytime adiabatic ML is a function of RH. Figure 8 compares summer observations from the Boreal Ecosystem Monitoring Study (BERMS) of daily-mean LW_n , binned by near-surface RH and cloud albedo with the nearest grid-point from ERA40 (Betts et al. 2006). The clear-sky fluxes from ERA40 are replicated on the left panel for BERMS. The time-periods are not the same, although they overlap; but the relationships are the same within the standard deviations shown for the variability of the daily data. Outgoing LW_n decreases as near-surface RH rises (and mean cloud-base falls), and decreases as cloud cover increases (represented here quantitatively by ECA). Here we see conceptually separated, the clear-sky LW_n water vapor greenhouse effect, and the LW_n cloud forcing, the greenhouse warming from cloud cover. At cold temperatures, when the solar zenith angle is low, such as in winter at high latitudes, the warming from the $LWCF_n$ dominates over the cooling from the $SWCF_n$ (see Canadian Prairie data in the next chapter).

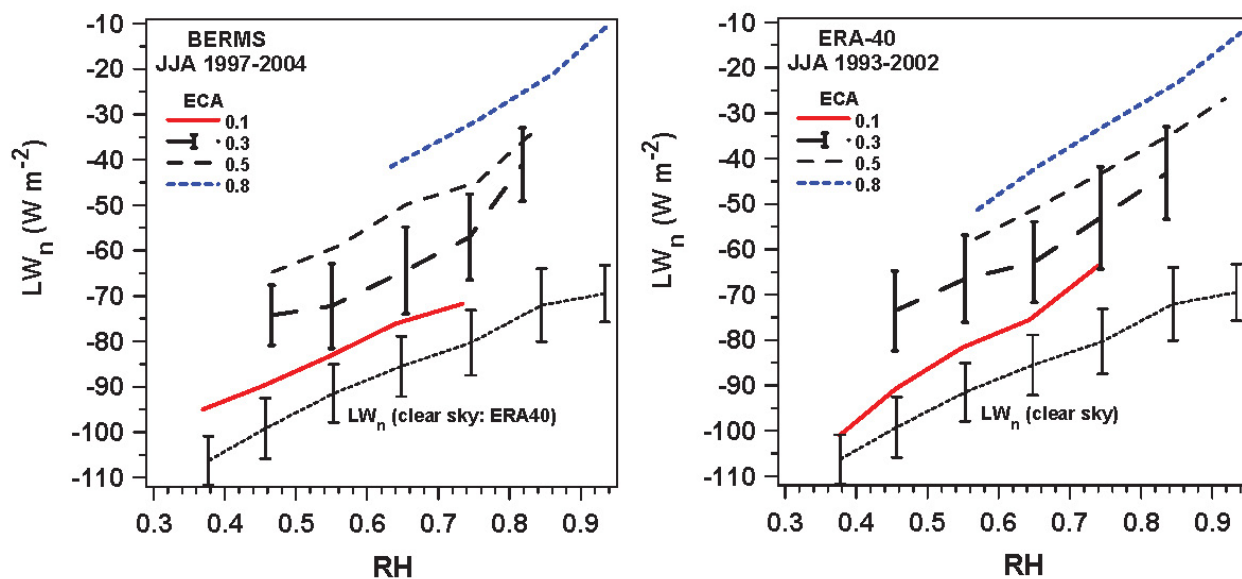


Figure 8. LW_n binned by daily mean 2-m RH and ECA for BERMS data and ERA-40 nearest grid-point. Standard deviations of the daily data shown only for clear-sky and one cloud albedo class. (Betts 2009)

Water availability and the surface energy partition

The storage of precipitation as soil water plays a critical role in the coupling between atmosphere and BL. Soil moisture is a strong constraint on evapotranspiration, and the availability of water primarily determines evaporative fraction: $EF = \lambda E / (\lambda E + H)$, where λE and H are the latent and sensible heat fluxes.

Figure 9 illustrates the primary role of soil water in the surface energy partition, and the impact on the diurnal cycle of 2-m temperature and humidity. Twenty-eight days with nearly clear skies during July and August, from the 1987 FIFE grassland prairie experiment near Manhattan, Kansas (Betts and Ball 1995, 1998) have been stratified into three roughly equal groups, based on the 0-10cm volumetric soil moisture (which was measured gravimetrically). The left panel shows the mean diurnal cycle of R_n (left-hand-scale) and daytime evaporative fraction EF (right-hand-scale). R_n is almost the same for each group of days, peaking around 615 W m^{-2} at local noon (about 1820 UTC), because the days were chosen for nearly clear skies. However the partition of R_n into λE and H , represented by EF is radically different. As mean soil moisture increases from 14.7% (when the vegetation is stressed) to 29.9% (when the vegetation is unstressed), near-noon EF increases from 0.54 to 0.75. The right panel shows the large impact of these different surface fluxes on the diurnal cycle of 2-m temperature, T , and relative humidity, RH . We see the typical mirror opposites of RH falling as T rises, because diurnal changes of mixing ratio are relatively small. However, with drier soils when the vegetation is stressed, there is a larger systematic shift to higher temperature and lower RH . From wet to dry soils, the afternoon RH minimum drops from 53% to 30%. This corresponds to an increase in P_{LCL} , the pressure height of the LCL above the surface, from 134 to 239 hPa in the afternoon.

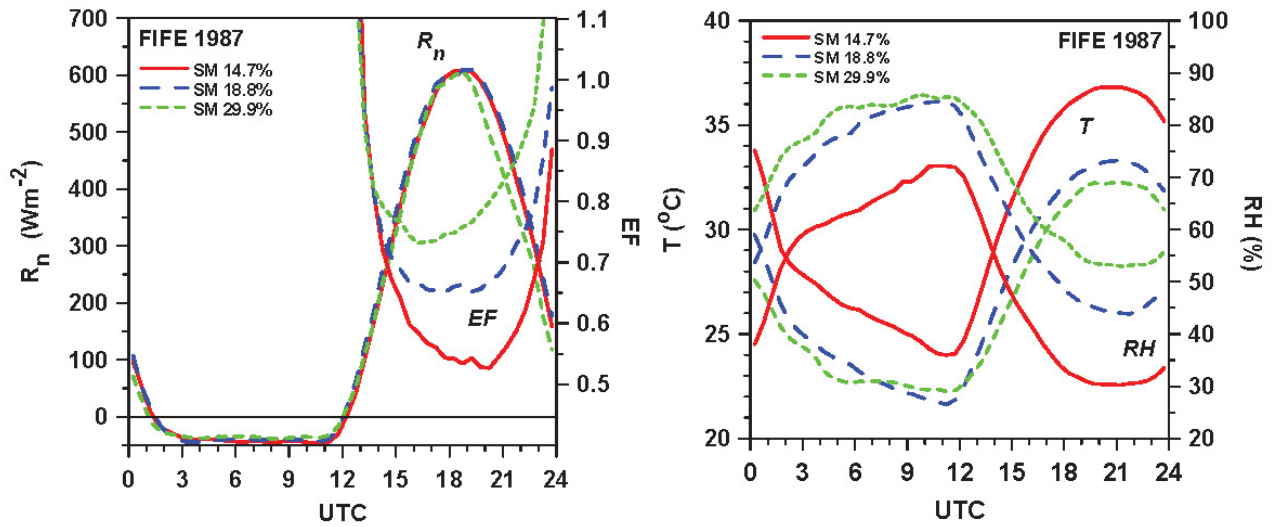


Figure 9. Diurnal cycle of R_n and EF (left) and 2-m temperature and RH (right) for FIFE summer composites. (Betts 2009)

Diurnal cycle on vector diagrams

Two-dimensional vector plots are helpful for visualizing and quantifying the balance of processes involved in the diurnal cycle (Betts 1992; Santanello et al. 2009). Figure 10 is a remapping from Figure 9 of the daytime 2-m diurnal cycle (from 1115 to 2245 UTC) for the three FIFE soil moisture composites into a conserved variable reference frame. The left panel is a (θ, Q) plot (potential temperature and mixing ratio): with a duplicate $(C_p\theta, \lambda Q)$ scale in J kg^{-1} . The right panel is the same data on a (θ_E, P_{LCL}) plot, where θ_E is equivalent potential temperature. The left panel has auxiliary dotted lines, corresponding to saturation pressure, $p^* = 900\text{hPa}$, and virtual potential temperature, $\theta_v = 298\text{K}$. The p^* isopleths are roughly parallel, so one can visualize the rise of LCL along the daytime surface trajectories on the (θ, Q) plot.

The triangle, superimposed on the left panel, is a schematic BL vector budget for the high soil moisture composite for the period 1415 to 2045: representing the vector time-change as the sum of a surface flux vector and an entrainment flux vector. This is constructed as follows (see Betts 1992). The simplified mixed layer (ML) budget can be written for a time-step, Δt , when the mean depth of the mixed layer is ΔZ_i , as

$$\Delta \xi_m / \Delta t = (\mathbf{F}_s - \mathbf{F}_i) / \rho \Delta Z_i \quad (6)$$

where $\Delta \xi_m$ is the vector $\Delta(C_p\theta, \lambda Q)_m$, that is, the change in ML values between 1415 and 2045 (heavy long dashes), \mathbf{F}_s is the surface flux vector and \mathbf{F}_i is the entrainment flux vector, representing the mixing down of warm, dry air from above the ML. We approximate the ML change with the 2-m change of $(C_p\theta, \lambda Q)$ in Figure 9. The length of the surface flux vector (heavy line) is calculated [setting $\theta/T \approx 1$] from the relation

$$\mathbf{F}_s = (H, \lambda E) = \Omega \Delta(C_p \theta, \lambda Q) \quad (7)$$

using the scaling ‘velocity’

$$\Omega = \rho \Delta Z_i / \Delta t \quad (8)$$

The entrainment vector, \mathbf{F}_i , is the third (dotted) leg of the triangle, which can be found as a residual, using (8) to convert the dotted vector to a flux. Thus the ML step from 1415 to 2045 can be regarded as the sum of the surface flux vector, which warms and moistens, and the entrainment vector that warms and dries the ML. We have of course ignored advection in the simplified Eq (6), so the advection of $(C_p \theta, \lambda Q)$ in time Δt is also a vector contribution to the residual. Warm, dry advection will have a similar impact on the ML as the entrainment of warm, dry air from above. Using a large time-step (here 6.5h) in (6) introduces a small approximation, but for the case shown it is only a few %. The slope of the surface flux vector on Figure 10 is related to the surface Bowen ratio, $BR = H/\lambda E$: it is actually $(\theta/T)(H/\lambda E)$, since the figure is plotted in terms of potential temperature. For this high soil moisture case, the surface flux vector is slightly less than the slope of $p^* = 900$ hPa, meaning that the surface fluxes alone would tend to lower cloud-base slightly. It is the entrainment fluxes therefore that are responsible for the rise of cloud-base. For this high soil moisture composite, we have an estimate of mixed layer depth, $\Delta Z_i(t)$, from sequential sondes (Betts and Ball 1994), launched during intensive periods. We do not show the corresponding vector figures for the drier soils, because there is no sonde data. However as EF falls, BR increases and the surface flux vector becomes steeper (that is, it rotates anti-clockwise), which contributes to the greater rise of P_{LCL} . In addition, entrainment of dry air from above the ML (which has a lower saturation pressure) also increases as H increases.

The right panel showing (θ_E, P_{LCL}) gives a reference for moist processes. Also shown (open circle) is the equilibrium state over a tropical ocean corresponding to the same daily mean surface flux, $H+\lambda E$, as these FIFE composites, from the solutions of Betts and Ridgway (1989); and the 24-h mean surface 2-m states for our FIFE composites (solid circles). The picture here is that, although the mean state over land has a lower θ_E than over the oceans, the superimposed diurnal cycle over land gives a higher θ_E in the afternoon; and the highest values (favoring deep convection) for the wettest soils for which evaporation is the highest. Afternoon cloud-base is the lowest over wet soils, although not as low as over the ocean, because of the impact of stomatal conductance/resistance in dropping RH below saturation across the leaf surface discussed earlier.

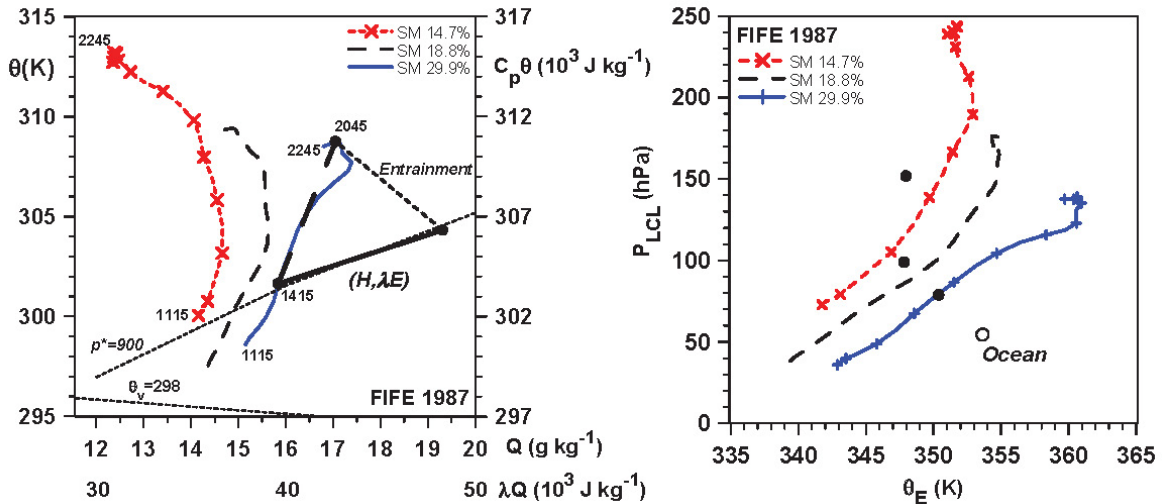


Figure 10. Daytime 2-m diurnal cycle for three FIFE composites, partitioned by soil moisture: (left) (θ, Q) plot, showing vector budget from 1415 to 2045 UTC, and (right) (θ_E, P_{LCL}) plot. (Betts 2009)

Land-surface-BL Coupling

In the coupled land-surface-BL system, evapotranspiration is just one factor. Figure 10 shows that the 24-h mean P_{LCL} shifts with the availability of water for evaporation, so it is useful to look at the relationships between daily mean parameters, even though the day and night-time boundary layers differ. The BL equilibrium of RH and LCL on daily timescales depends on atmospheric processes as well as surface processes.

Figure 11 shows for ERA40 for the Madeira river the joint dependence of P_{LCL} (with RH plotted on right-hand-scale with slight approximation) binned by precipitation rate (in mm/day) and first-layer (0-7cm) soil moisture

index, SMI-L1 (left panel) and EF (right panel). SMI-L1 is not only a useful index on the daily time-scale for the availability of water for evaporation (although transpiration depends also on soil water in deeper layers), but it also responds to precipitation on this time-scale. A representative set of standard deviations of the daily mean data are shown. Not surprisingly as SMI and EF increases, mean cloud base descends and RH increases; but RH also increases as precipitation increases. This is a highly coupled system. When the LCL is lower, more precipitation is likely; but the converse is also true: the evaporation of precipitation as it falls through the sub-cloud layer will lower the LCL, and increase SMI-L1 on daily time-scales.

Figure 11 links one key *observable* (P_{LCL}) with several important but poorly measured processes in the land-surface-atmosphere coupling. Over the diurnal cycle of the boundary layer the atmosphere integrates over much larger spatial scales, so that the diurnal cycle of P_{LCL} and its daily mean represent processes on scales of order one day's advection (345 km at 4 m s^{-1}). Soil moisture is an important parameter in the model system, but in the real world, in-situ measurements of soil moisture represent quite local processes. Satellite microwave measurements may give us useful estimates of near-surface soil moisture. EF can be measured on towers, but these are representative only of a local footprint. On basin-scales we can make estimates of the land-surface fluxes using hydrologic models (Maurer et al., 2002). Evaporation of falling precipitation plays a fundamental role in the model surface interaction, because evaporation of water above the surface cools and moistens the BL, which increases the surface Bowen ratio; while evaporation off a wet canopy reduces the Bowen ratio. The structure shown in Figure 11 for ERA40 is broadly consistent with observations, but models in general show a wide range of behavior (Dirmeyer et al. 2006).

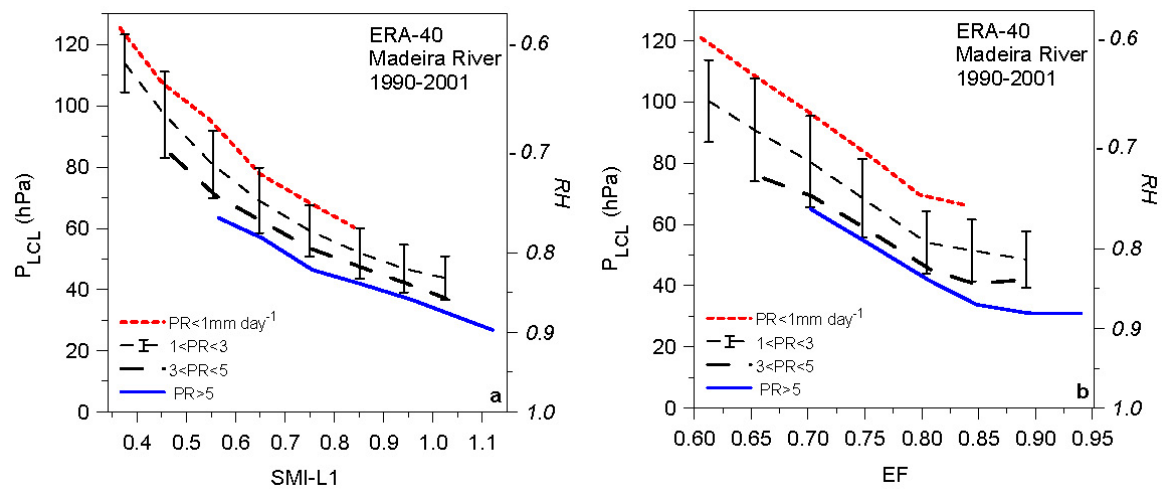


Figure 11. Stratification of P_{LCL} by soil moisture index and precipitation (left) and (right) EF and precipitation. Daily-mean ERA-40 data for Madeira River. (Betts 2009)

Separating cloud and surface controls on the SEB and EF

Figure 12 shows a conceptual split of the surface energy balance in terms of the atmospheric and cloud processes that primarily determine R_n ; and the surface processes, soil moisture and temperature that primarily determine EF (the partition of R_n). We use ERA40 data, averaged over the Missouri river basin (Betts 2007), so the figures reflect the physical parameterizations in that reanalysis.

The left panel is the partition of R_n into the clear-sky R_n (clear) and the net cloud forcing $CF_n = SWCF_n + LWCF_n$.

$$R_n = R_n(\text{clear}) + CF_n \quad (9)$$

We have chosen May-August, so the variations in the top-of-the-atmosphere solar flux are small. We have added the partition with soil moisture, SMI-L1, but this has almost no impact on CF_n and little impact on R_n (clear). Surface albedo, not shown, has little variability in summer. So we can think of surface R_n being the sum of the clear-sky flux with little variability in summer, and the atmospheric cloud forcing, which has a quasi-linear dependence on ECA. EF shown in the right panel determines the partition of R_n ; and this is a strong function of soil moisture, represented here by SMI-L1, but also of temperature. The slope with temperature is close to the slope of the classic 'equilibrium evaporation' relation [Priestley and Taylor 1972; McNaughton 1976], defined as

$$EF^* = \beta/(1+\beta) \quad (10)$$

where $\beta(T) = (\lambda/C_p) (\partial q_s/\partial T)_p$ is related to the slope of the Clausius-Clapyron equation at constant saturation pressure, plotted here for the mean surface pressure, 900hPa for the Missouri river basin. The slope of (10) on Figure 12 just comes from the non-linearity of the Clausius-Clapyron equation. There are of course many other non-linear processes influencing the surface fluxes in the model (ERA40), but we can loosely interpret the right panel as conceptually splitting the thermodynamic impact of increasing temperature on EF (at constant p^*) from the impact of decreasing soil moisture (and increasing vegetative resistance), which by dropping the RH across the leaf, reduces mixed layer RH and p^* , and increases P_{LCL} and mean cloud-base.

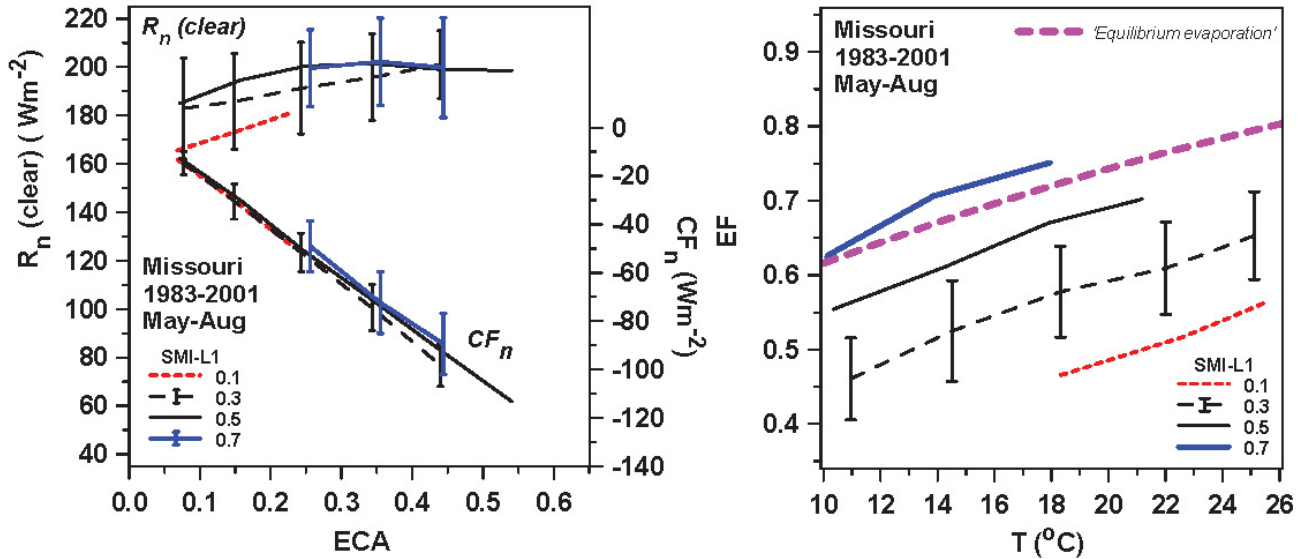


Figure 12. Dependence of R_n (clear-sky) and cloud forcing on ECA (left) and (right) EF on temperature and soil moisture index. (Betts 2007)

Relation of cloud SW forcing to precipitation forcing

For the Mississippi basin, the data is sufficient to assess the ratio of the surface SWCF_n and the diabatic forcing of the atmosphere by precipitation. This ratio is critical to the climate of a model system, as it is a measure of the impact of clouds on the energy partition between atmosphere and the surface, since precipitation heats the atmosphere, while the SW cloud forcing cools the surface. Figure 13 for the Missouri river basin (Betts 2007), bins 19 years of daily mean warm season precipitation by ECA and P_{LCL} . The left panel is from ERA40 and the right uses ECA from ISCCP and gridded precipitation from the Higgins et al. (2000) dataset. ERA40 P_{LCL} has been used to stratify both, because it is somewhat constrained by a surface humidity analysis. For a given cloud albedo, ERA40 has more precipitation. Converting precipitation to energy units, the ratio of the SWCF_n to the diabatic precipitation forcing is 0.48 for ERA40 and 0.74 for the observations for $P_{LCL} = 60$ hPa (Betts 2007). So from a climate perspective, for a given heating of the atmosphere by precipitation (which is constrained by the large-scale dynamics), the SW cooling of the surface in ERA40 is too small. Note that in the observations the radiative impact of clouds and their diabatic impact from precipitation are comparable in magnitude. This is generally true on all timescales in the atmosphere; and it means that the radiation field plays a tightly coupled role in the vertical transports by the cloud field. Often, however, this coupling may not be properly represented in models.

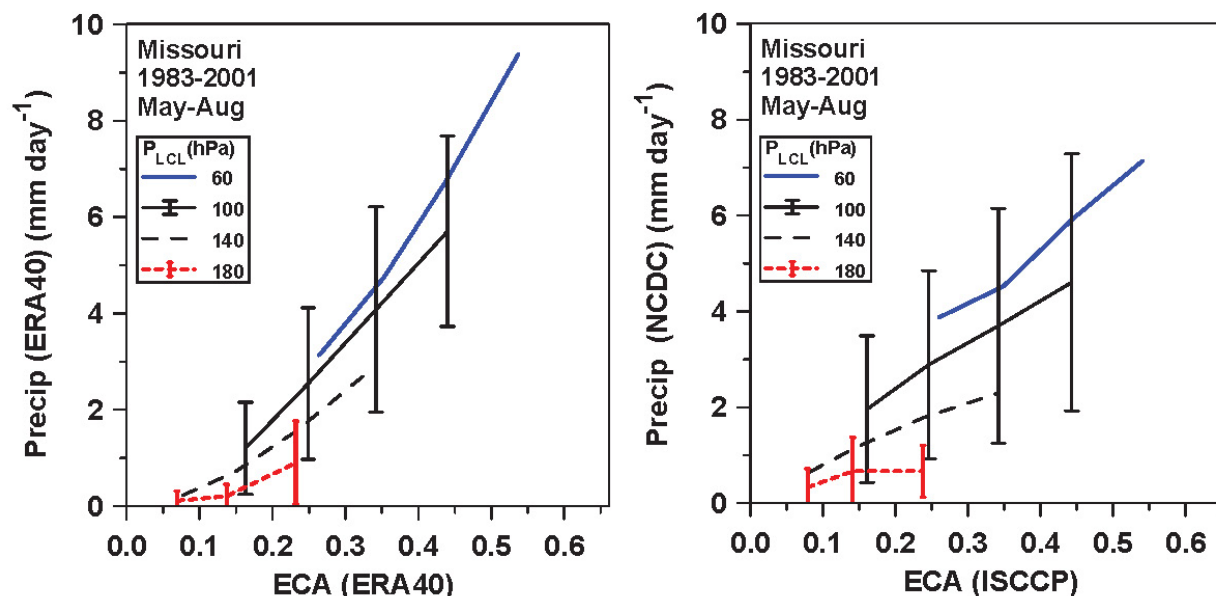


Figure 13 Warm season precipitation for the Missouri river basin stratified by ECA and P_{LCL} for ERA40 (left) and (right) NCDC and ISCCP observations. (Betts 2007)

Summary

These Figures have been taken from two review papers (Betts 2004, 2009) to illustrate some of the basic physical processes and links that can be seen in observations and models at the land-surface. My framework is both diagrammatic and conceptual; looking for relationships and information in the coupling of processes and observables from a systems perspective. Models have only limited value if we do not have a deep understanding of the coupling of processes within the model system; and observations are important both for evaluation, and to suggest important processes that are simply missing.

We have made heavy use of ERA40 reanalysis data both because we have a full suite of variables and because the data assimilation constrains the short term forecasts. However the land surface solutions depend on many highly coupled parameterized processes: for the soil model, vegetation model, surface and BL models, cloud, precipitation and radiation parameterizations. The next chapter takes an observational perspective of land-atmosphere-cloud coupling using the remarkable climate station data from the Canadian Prairies.

Acknowledgement

This research was supported by the National Science Foundation and the National Aeronautics and Space Administration.

REFERENCES

- Beljaars, A.C.M., Viterbo, P., Miller, M.J., and Betts, A.K. (1996). The anomalous rainfall over the United States during July 1993: sensitivity to land surface parameterization and soil moisture anomalies. *Mon. Wea. Rev.*, 124, 362-383.
- Betts, A. K. 1982. Saturation Point Analysis of Moist Convective Overturning. *J. Atmos. Sci.*, 39, 1484-1505.
- Betts, A.K. 1992. FIFE Atmospheric Boundary Layer Budget Methods. *J. Geophys. Res.*, 97, 18523-18532.
- Betts, A. K. 2000. Idealized model for equilibrium boundary layer over land. *J. Hydrometeorol.*, 1, 507-523.
- Betts, A. K. 2004. Understanding Hydrometeorology using global models. *Bull. Amer. Meteorol. Soc.*, 85, 1673-1688.
- Betts, A. K. 2007. Coupling of water vapor convergence, clouds, precipitation, and land-surface processes, *J. Geophys. Res.*, 112, D10108, doi:10.1029/2006JD008191.

- Betts, A. K. 2009. Land-surface-atmosphere coupling in observations and models. *J. Adv. Model Earth Syst.*, Vol. 1, Art. #4, 18 pp., doi: 10.3894/JAMES.2009.1.4
<http://james.agu.org/index.php/JAMES/article/view/v1n4/JAMES.2009.1.4>
- Betts, A.K. and W. L. Ridgway 1989. Climatic equilibrium of the atmospheric convective boundary layer over a tropical ocean. *J. Atmos. Sci.*, 46, 2621-2641.
- Betts, A.K. and J.H. Ball 1994. Budget analysis of FIFE-1987 sonde data. *J. Geophys. Res.*, 99, 3655-3666.
- Betts, A.K. and J.H. Ball 1995. The FIFE surface diurnal cycle climate. *J. Geophys. Res.* 100, 25679-25693.
- Betts A. K. and J. H. Ball 1997. Albedo over the boreal forest. *J. Geophys. Res.*, 102, 28901-28910.
- Betts A. K. and J. H. Ball 1998. FIFE surface climate and site-average dataset: 1987-1989. *J. Atmos Sci* , 55, 1091-1108.
- Betts, A. K. and J. C. Chiu 2010. Idealized model for changes in equilibrium temperature, mixed layer depth and boundary layer cloud over land in a doubled CO₂ climate. *J. Geophys. Res.*, 115, D19108, 2009JD012888.
- Betts, A. K., J.H. Ball, A.C.M. Beljaars, M.J. Miller and P. Viterbo 1996. The land-surface-atmosphere interaction: a review based on observational and global modeling perspectives. *J. Geophys. Res.* 101, 7209-7225.
- Betts, A. K., J.H. Ball and P. Viterbo 1999. Basin-scale surface water and energy budgets for the Mississippi from the ECMWF Reanalysis. *J. Geophys. Res.*, 104, 19293-19306.
- Betts, A. K., M. L. Goulden, and S.C. Wofsy 1999. Controls on evaporation in a boreal spruce forest. *J. Climate*, 12, 1601-1618.
- Betts, A. K., J. H. Ball, and J. H. McCaughey 2001. Near-surface climate in the boreal forest. *J. Geophys. Res.*, 106, 33529-33542.
- Betts, A. K., B. Helliker and J. Berry 2004. Coupling between CO₂, water vapor, temperature and radon and their fluxes in an idealized equilibrium boundary layer over land. *J. Geophys. Res.*, 109, D18103, doi:10.1029/2003JD004420.
- Betts, A.K., J. Ball, A. Barr, T. A. Black, J. H. McCaughey and P. Viterbo 2006. Assessing land-surface-atmosphere coupling in the ERA-40 reanalysis with boreal forest data. *Agricultural and Forest Meteorology*, 140, 355-382, doi:10.1016/j.agrformet.2006.08.009.
- Dirmeyer, P. A., R. D. Koster, and Z. Guo 2006. Do global models properly represent the feedback between land and atmosphere? *J. Hydrometeor.* 7, 1177-1198, doi:10.1175/JHM532.1.
- Higgins, R. W., W. Shi, E. Yarosh, R. Joyce 2000. Improved United States Precipitation Quality Control System and Analysis, NCEP/Climate Prediction Center ATLAS No. 7, U. S. Department of Commerce, National Oceanic and Atmospheric Administration, National Weather Service.
- Maurer, E.P., A.W. Wood, J.C. Adam and D.P. Lettenmaier 2002. A long-term hydrologically based dataset of land-surface fluxes and states for the conterminous United States. *J. Climate*, 15, 3237-3251, doi:10.1175/1520-0442(2002)015<3237:ALTHBD>2.0.CO;2.
- McNaughton, K. G. 1976. Evaporation and Advection I: Evaporation from Extensive Homogeneous Surfaces, *Quart. J. Roy. Meteorol. Soc.* 102, 181-191.
- Priestley, C. H. B. and Taylor, R. J. 1972. On the Assessment of Surface Heat Flux and Evaporation, *Mon. Wea. Rev.* 106, 81-92.
- Santanello, J. A., C. D. Peters-Lidard, S. V. Kumar, C. Alonge and W-K. Tao 2009. A Modeling and Observational Framework for Diagnosing Local Land-Atmosphere Coupling on Diurnal Time Scales. *J. Hydrometeor.*, 10, 577-599. doi: <http://dx.doi.org/10.1175/2009JHM1066.1>
- Van den Hurk, B.J.J.M., P. Viterbo, A.C.M. Beljaars and A. K. Betts 2000. Offline validation of the ERA40 surface scheme. *ECMWF Tech Memo*, 295, 43 pp., Eur. Cent. For Medium-Range Weather Forecasts, Shinfield Park, Reading RG2 9AX, England,UK.
- Viterbo, P. and A.K. Betts 1999. The impact on ECMWF forecasts of changes to the albedo of the boreal forests in the presence of snow. *J. Geophys. Res.*, 104, 27 803-27 810.

ABOUT THE AUTHOR

Alan Betts: Dr. Alan Betts of Atmospheric research in Pittsford, Vermont, USA is an independent climate scientist. He is a Fellow of the American Geophysical Union, the American Meteorological Society (AMS), the Royal Meteorological Society, the American Association for the Advancement of Science, and a past-president of the Vermont Academy of Science and Engineering. He is the author or co-author of more than 165 reviewed papers in the scientific literature. He was the AMS Robert E. Horton Lecturer in Hydrology in 2004; and the AMS Jule Charney Award winner in 2007. His research, public lectures and articles are available at alanbetts.com.